



**HAL**  
open science

## New protective coatings against liquid zinc corrosion

Aleksandra Cieplak, Asma Gdoura, Bruno Gay, Leo Portebois, Nicolas Ramenatte, Ingrid Proriot Serre, David Balloy

### ► To cite this version:

Aleksandra Cieplak, Asma Gdoura, Bruno Gay, Leo Portebois, Nicolas Ramenatte, et al.. New protective coatings against liquid zinc corrosion. SN Applied Sciences, 2023, 5 (5), pp.142. 10.1007/s42452-023-05319-6 . hal-04078825

**HAL Id: hal-04078825**

**<https://hal.univ-lille.fr/hal-04078825>**

Submitted on 24 Apr 2023

**HAL** is a multi-disciplinary open access archive for the deposit and dissemination of scientific research documents, whether they are published or not. The documents may come from teaching and research institutions in France or abroad, or from public or private research centers.

L'archive ouverte pluridisciplinaire **HAL**, est destinée au dépôt et à la diffusion de documents scientifiques de niveau recherche, publiés ou non, émanant des établissements d'enseignement et de recherche français ou étrangers, des laboratoires publics ou privés.



Distributed under a Creative Commons Attribution 4.0 International License



# New protective coatings against liquid zinc corrosion

Aleksandra Cieplak<sup>1</sup> · Asma Gdoura<sup>2</sup> · Bruno Gay<sup>3</sup> · Léo Portebois<sup>4</sup> · Nicolas Ramenatte<sup>4</sup> · Ingrid Proriot Serre<sup>1</sup> · David Balloy<sup>1</sup>

Received: 2 December 2022 / Accepted: 21 February 2023

Published online: 19 April 2023

© The Author(s) 2023 [OPEN](#)

## Abstract

Hot dip galvanizing is a surface treatment used to form a corrosion-resistant layer on the surface of steel by dipping it in a liquid zinc bath. However, a lot of structures used for hanging or containing the parts during the process are made of steel and suffer from liquid zinc corrosion. Furthermore, Fe–Zn intermetallics formed on the surface induce an additional pickling and zinc consumption, therefore generating supplementary economic and environmental costs. In this article, two Fe–Cr–Ni–Si coatings synthesized by the slurry process on carbon steel (C22) were characterized by XRD, EDX, EPMA and EBSD analyses. Their corrosion protective properties were studied in the process imitating cyclic batch galvanizing and compared to those of uncoated carbon steel (C22) and stainless steel (316 L). The coatings were verified to be more efficient than the 316 L steel usually used for this application. After 9 cycles of no weight loss, molten zinc corrosion was linear and the same for Fe–Cr–Ni–Si coatings as for the stainless steel.

## Article highlights

Two Fe–Cr–Ni–Si coatings were synthesized by the slurry process on carbon steel (C22).

Their corrosion resistance in zinc bath is better to those of the 316 L steel.

**Keywords** Batch galvanizing · Molten zinc corrosion · Slurry process

## 1 Introduction

Hot dip galvanizing is a well-known surface treatment for steels to improve their atmospheric corrosion resistance. Steel parts are dipped in a molten zinc base alloy at around 450 °C for several minutes in order to form a protective coating. However, a lot of steel structures used for hanging or containing the parts during the dipping, undergo a corrosion by the liquid zinc alloy. Moreover, a zinc coating is formed on these structures that leads to an unnecessary

zinc consumption and a stripping step before their reuse. This step produces highly charged zinc solutions and supplementary economic and environmental costs (solution transport and treatment, loss of zinc).

The subject of surface reactivity in zinc bath alloys has already mainly been studied in the case of sink rolls and stabilizing rolls used in the continuous galvanizing process or in the case of a kettle containing the liquid zinc alloy [1–9]. Ceramics present a very good resistance to liquid zinc alloy corrosion and low wettability. In the continuous

✉ Aleksandra Cieplak, [aleksandra.cieplak@univ-lille.fr](mailto:aleksandra.cieplak@univ-lille.fr); ✉ David Balloy, [david.balloy@univ-lille.fr](mailto:david.balloy@univ-lille.fr) | <sup>1</sup>Univ. Lille, CNRS, INRAE, Centrale Lille, UMR 8207 - UMET - Unité Matériaux et Transformations, F-59000 Lille, France. <sup>2</sup>National Institute of Applied Sciences and Technology (INSAT), Carthage University, BP 676, 1080 Tunis Cedex, Tunis, Tunisia. <sup>3</sup>B.Circle, 2 Clos de 3 Couleurs, B-1150 Brussels, Belgium. <sup>4</sup>EEIGM, Université de Lorraine, 6 rue Bastien Lepage, 54010 Nancy Cedex, France.



galvanizing industry, a lot of vessels containing the liquid alloy are made in ceramics. However, in the batch galvanizing industry, for the hanging structures, ceramics are too brittle to be used because of very different thermal expansion coefficients between ceramic and steel.

In the case of continuous galvanizing, the rollers are continuously in contact with the liquid zinc alloy. Dross particles form at the surface and can print defects on the steel plate during its galvanizing. The main material used to limit liquid zinc corrosion is the stainless steel, eventually coated with WC–Co, but several studies report new materials or coatings [9, 10].

Several recent studies report new bulk materials with an improved behavior in contact with a liquid zinc alloy [8, 11]. Fe–Cr–Ni–B; Fe–Cr–Ni–Mo–B with 8 and 18 wt% Cr, up to 1 wt% Mo and 3.5 wt% B were investigated at 520 °C and present a corrosion resistance depending on the Cr and Ni content [8]. A mechanism of preferential dissolution of Cr and Ni and a spalling of boride was presented. The morphology of a directional microstructure was investigated by Wang Y. et al. for a material with 3.5 wt% B and compared to 316 L stainless steel [11]. They have also studied the effect of the temperature between 460 and 550 °C [12] and the wear behavior [13]. They show that a boride layer perpendicular to the interface (that means to the diffusion flow of zinc) inhibits the diffusion and slowdown the erosion-corrosion in liquid zinc alloy containing 0.3 wt% Al. Wang W.J. et al. [14] have studied the static isothermal corrosion of Fe<sub>3</sub>Si, Fe<sub>3</sub>Al and Ni<sub>3</sub>Al in liquid zinc at 450 °C compared with 316 stainless steel. The three intermetallics exhibited a lower resistance than the stainless steel and the corrosion was controlled by the dissolution in the liquid zinc. Considering the Fe<sub>3</sub>Si alloy, containing 16 at.% Si, 3 at.% Al, 1 at.% Ti, 1 at.% Ni, the authors report the formation of an Al and Si rich corrosion layer at the surface, with a thickness of 4 μm, that acts as a diffusion barrier. It was not possible to these authors to measure the exact composition of this layer and its extreme surface.

Fang et al. [15] have studied a Fe–21Cr–9Mn–4Ni–2Nb (wt%) materials modified by a surface treatment like nitriding and/or oxidizing. This alloy exhibited a very good corrosion resistance in continuous dipping for more than 25 days, by the formation of a corrosion resistant and unwettable oxide layer. The nitridized layer shows a longer incubation time than the oxidized one.

Considering metallic coatings, in some industrial applications a composite coating constituted of WC particles in a Co base matrix deposited by high velocity oxygen fuel (HVOF) is used. This coating is thin and expensive, applied by thermal projection and has to be regularly recharged. This solution is clearly not adapted to the context of hot-dip batch galvanization [16]. Zhang et al. have compared the behavior of WC–Co coatings with new MoB–CoC ones

[10]. Results showed that MoB–CoCr coating exhibited better resistance property to thermal shock than that of WC–12Co. At the same time, the corrosion test showed that life-time of coated samples by MoB–CoCr appeared to be longer than WC coating. This behavior is ascribed to non-wettability of MoB–CoCr coating limiting the molten zinc penetration along the micro-cracks present in the coating.

When compared to thermal spray coatings, diffusion coatings are of interest for reducing the quantity of metallurgical defects but also for improving the thermo-mechanical resistance of systems [17]. Among them, in situ chemical vapor deposition (CVD) by the pack cementation technic is widely used at industrial scale to increase the Al [18], Cr [19] or Si [20] or a mix [21] surface content of various substrates. However, main applications of this process concern quite high added value parts for sectors such as aeronautics, aerospace or energy, which is far away from the global galvanization market.

An alternative to produce metallic coatings is the fused slurry process. Developed in the 60s by Priceman et al. [22], this technique is very attractive to coat large components with complex shapes, thanks to its versatility. Indeed, the fusible precursor containing the element to deposit (elemental or prealloyed) is mixed with liquid phase, ethanol and water being the most used, and various products can be added to modify the surface tension and/or the viscosity of the liquid [23]. Then, the slurry is applied by spraying, dipping or brushing and heat treated in controlled atmosphere. Regarding the wetting ability of molten metallic alloys, it is possible to achieve very uniform coating with a high reliability, at reasonable costs.

This article presents the results of the study on two coatings obtained by slurry process exposed to corrosion applied by the galvanizing process. The hanging structures undergo a cyclic dissolution through the Fe–Zn intermetallics formation followed by the stripping in acid after each galvanizing cycle. Therefore, to reproduce this phenomenon, similar surface treatment as in batch galvanizing was applied during 20 cycles and the corrosion was quantified by part's weight loss after each stripping. Those coated samples' corrosion resistance was compared with 316 L steel used as pot roll material [2].

## 2 Experimental

### 2.1 Steel compositions

Chemical compositions of the carbon steel C22 and stainless steel 316 L used in this study are reported in the Table 1. The 316 L was supplied by Aperam and its composition was obtained by sequential X-ray fluorescence. Steel samples are rods with 12 mm diameters and 70 mm length.

**Table 1** Composition (in weight% - balance: iron) of the 2 steels: C22 and 316 L

C22 (wt%)	C	Si	Mn	P	S	Cr	Mo	Ni	Cr+Mo+Ni
	0.17–0.24	<0.40	0.40–0.70	<0.045	<0.045	<0.40	<0.10	<0.40	<0.63
316 L (wt%)	C	Co	Cr	Cu	Mn	Mo	Nb	Ni	
	<0.02	0.14	18.08	0.34	1.52	0.24	0.017	8.13	
	P	Si	Sn	Ta	Ti	V	W	Zr	
	0.029	0.33	0.009	0.005	0.001	0.11	0.098	0.003	

**Table 2** Global compositions (wt%) of the slurries

Element	Concentration (wt%)	
	Composition A	Composition B
Ni	74.3	57.0
Cr	9.3	28.5
Fe	2.1	
Si	12.9	8.8
B	1.4	
P		5.7

## 2.2 Coating procedure

Two Fe–Cr–Ni–Si coatings were synthesized to coat the C22 steel by slurry. The difference between the 2 coatings is the composition of the used slurries, especially in iron, boron and phosphorus.

The first step of the slurry process consists in mixing pure elements and commercial prealloyed powders to obtain two global compositions given in Table 2. All particle sizes were inferior to 100 µm. A Turbula T2-F shaker-mixer is used for 2 h in order to achieve a homogenous mixing. Powders are then dispersed in a binder aqueous solution prepared by dissolving 12 wt% polyvinyl alcohol (PVA) in distilled water and mixed here again in the Turbula T2-F shaker-mixer for 1 h.

C22 steel rods surfaces are ground using P240 and P600 SiC papers and ultrasonically cleaned in acetone at room temperature. Both compositions' slurry is applied by a dip coating process with the same, constant withdrawal rate of around 1 mm/s and air dried before being heated in an industrial TAV THF 80/80/250 vacuum furnace. Thermal cycle consists in one debinding step at 350 °C and a high temperature 10 min step at 1040 °C for both compositions. Heating ramp equals 10 °C.min<sup>-1</sup>. Operating vacuum is close to 10<sup>-5</sup> mbar and cooling is slow, provided by the inertia of the furnace.

The 2 coated C22 steels synthesized from the slurries with the composition A and the composition B are noted coating A and coating B respectively.

## 2.3 Microstructure characterization

The material characterization of the coated C22 steel was carried out on the electron microscopy facility and on the XRD platform of the Advanced Characterization Platform of the Chevreul Institute. Indeed, the microstructure of the coated steel was observed with a scanning electron microscope (SEM, JEOL JSM-7800 F LV) and analyzed with energy dispersive X-ray spectrometer (EDX, Bruker - Quantax). EDX results presented in this paper are the average values of almost 5 punctual analyses with the standard deviation in the order of magnitude of 5 at.%. Later, the chemical composition was analyzed with electron probe microanalyzer (EPMA, Cameca SX100) for more precision. All the elements were calibrated with pure metals, except for B for which the NB standard was used. EPMA results are the average values of 2 punctual analyses. Crystal structures of both samples were also characterized by X-ray diffraction (XRD, Rigaku Smartlab) in Bragg-Brentano geometry, with Cu Kα radiation (λ = 1.54 Å). The phase attribution was confirmed by the Electron Backscatter Diffraction (EBSD, SEM Hitachi SU5000 with Oxford Symmetry EBSD camera).

## 2.4 Corrosion tests in liquid zinc alloy

Corrosion resistance test was realized in order to reproduce what the hanging structures sustain during the hot dip batch galvanizing. In this cyclic test, samples underwent at each cycle the steps chosen accordingly to the galvanizing process. First, the samples were stripped in HCl (15%) bath with 2% hexamethylenetetramine corrosion inhibitor until total removing of the zinc coating. After rinsing in water and drying in oven at 110 °C, a weight measurement was carried out (the considered value is the average value of 20 measurements by sample). Then, the samples were fluxed in ZnCl<sub>2</sub> (280 g.l<sup>-1</sup>) + NH<sub>4</sub>Cl (220 g.l<sup>-1</sup>) aqueous salts flux, and after dried in oven at 110 °C for at least 10 min. The galvanizing for 3 min in a 10-litter bath of liquid zinc-based alloy (EN 1461) at 450 °C +/- 2 °C was performed. Finally, the samples were cooled at room temperature in ambient air.

2 samples of carbon steel, 2 samples of stainless steel, 1 sample of steel with A coating and 1 sample of steel with B

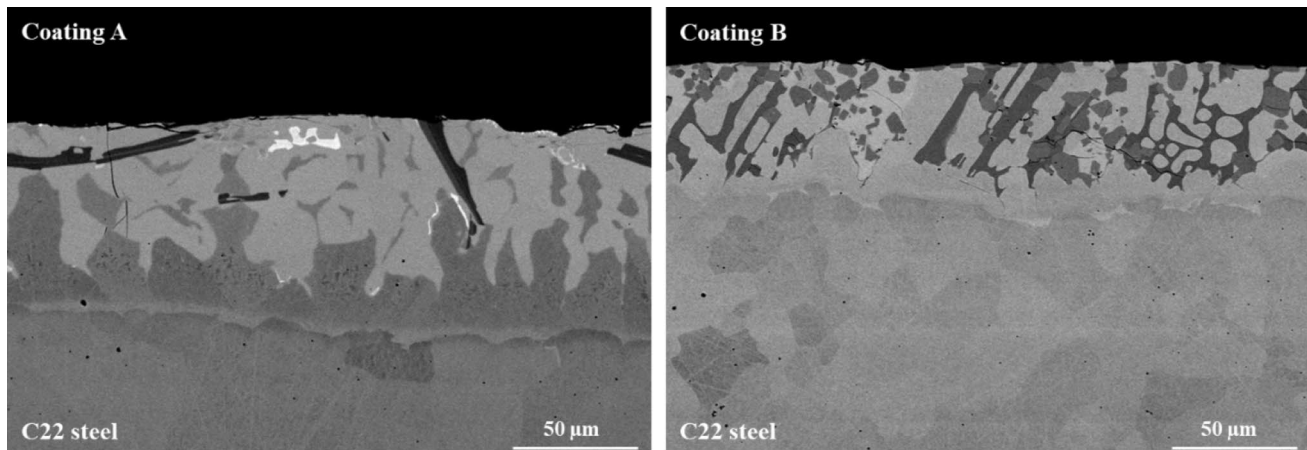


**Fig. 1** SEM observations of a cross section of the coatings A and B with the substrate (C22 steel)

coating were tested in cyclic galvanizing test for a cumulative residence time of 60 min (20 cycles of 3 min).

### 3 Results

#### 3.1 Microstructure characterization

The microstructures of the C22 steel with the coating A and with the coating B observed by SEM are presented on Fig. 1.

The thicknesses of the coatings presented on Fig. 1 are different, with a value between 70 and 90 μm and between 40 and 55 μm respectively for the coating A and the coating B.

The microstructure of the coatings is very complex with numerous phases. On both coatings, cracks are observed (Fig. 1): at the surface and in the light grey phase in coating A and in the lightest and the darkest phases in coating B. However, in both cases, cracks propagation seems to be stopped by the phase close to the steel. The EDX analysis of phases are given in Figs. 2 and 3; Table 3. For the coating A, phase A1, in light gray on Fig. 2, presents a composition with a high content in Si (17.6 at.%), Ni (18.5 at.%), Fe (55.5 at.%) and Cr (7.0 at.%). Phase A2 presents a similar composition with Si (12.6 at.%) Ni (17.7 at.%), Fe (61.2 at.%) and Cr (7.6 at.%). These two phases are Fe rich probably due to the iron diffusion from the steel during the slurry process. The difference in the color contrast may result from the slight difference in Ni and Cr contents. Phases A3 and A4, in black, present also a composition very close with very high concentration in B (22–24 at.%) and Cr (36–37 at.%). EDX analysis of phase A5, in white, shows the presence of Nb (2.1 at.%), Mo (9.0%), V (2.6 at.%), but also of Fe (28 at.%), Si (15.6 at.%), Cr (21.3 at.%) and Ni (21.1 at.%) in high proportions. Finally, the dark gray islands in the A2 phase,

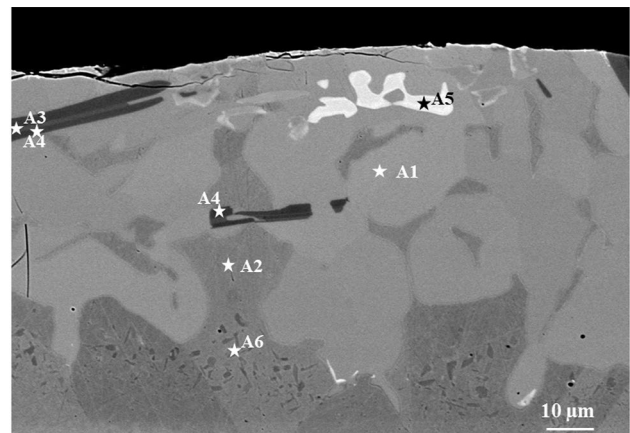


**Fig. 2** Different phases in coating A, according to EDX analysis in Table 3

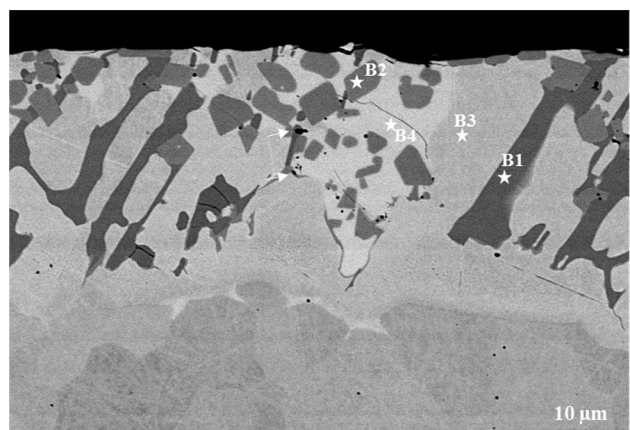


**Fig. 3** Different phases in coating B, according to EDS analysis in Table 3

**Table 3** EDX composition (at.%) of the phases observed on coating A and coating B (according to Figs. 2 and 3)

Phase	O	Al	Si	P	Cr	Mn	Fe	Ni	Mo	V	B	Nb
A1			17.6		7.6	0.1	55.5	18.5	0.4	0.2		
A2			12.6		7.0	0.2	62.1	17.7	0.2			
A3					37.2	0.3	38.0	1.1	0.6	0.6	22.1	
A4					36.7	0.3	36.6	1.0	0.7	0.6	24.1	
A5			15.6		21.3	0.2	28.0	21.1	9.0	2.6		2.1
A6			14.9		2.4	0.1	59.9	15.3			7.4	
B1			0.4	26.5	33.3	0.2	15.4	20.6				
B2			13.4	2.0	48.6	0.3	3.7	32.0				
B3			11.0		13.8	0.2	34.1	40.8				
B4			17.7	6.0	13.0	0.2	11.3	51.8				
Black dots	22.6	2.2	18.6	8.5	14.7	0.1	13.0	20.3				

called the phase A6 presents a relatively high content in B (7.4 at.%) and Si (14.9 at.%), with Ni (15.3 at.%) and a high content of Fe (59.9 at.%).

For the coating B, the very dark phase in Fig. 3, B1, shows a very high content in P (26.5 at.%), Cr (33.3 at.%), Ni (20.6 at.%), in addition with 15.4% at. Fe. The phase B2, in dark gray, presents a very high content in Cr (48.6 at.%), Ni (32 at.%) and Si (13.4 at.%). B3 phase, in contact with the steel matrix shows the highest content in Fe (34.1 at.%) with a lot of Ni (40.8 at.%) and a high content in Cr (13.8 at.%) and Si (11 at.%). The B4 phase, in light gray, shows the highest content in Si (17.7 at.%) with P (6 at.%), Cr (13.0 at.%), Fe (13.0 at.%) and a matrix of Ni (51.8 at.%). B1 and B3 phases presents a coarse eutectic like microstructure.

The EPMA analysis of phases is given in Table 4. The composition of the phases is close in term of the order of abundance of each element per phase, but not identical regarding the numerical value of the EDX results. The most differences can be observed in the coating (A) First of all, no clear distinction between phases A3 and A4 was observed with EPMA. Also, several grains of the rare A5 phase were analyzed. It was observed, that those are inclusions rich in Nb and Mo that vary significantly in their composition. Furthermore, another type of inclusions was observed near the surface and in proximity of A3 phases. Those inclusions were rich in B and Mo. Mo and Nb were

not intentionally introduced into the coating and may come from the steel. Moreover, A6 shows no presence of (B) Concerning the coating B, no black dots were observed and the values for other phases are close to EDX results. Both analyses let to characterize the composition of all principal phases present in the coatings.

### 3.2 XRD phase identification

The Fig. 4 presents the XRD patterns of the two coatings.

Only four phases were identified for the coating A (Fig. 4a). The most intense A1 phase correspond to  $\pi$ -ferrosilicide ( $P2_13$ ,  $a = 6.17 \text{ \AA}$ ) [24]. A2 phase could be identified as FCC  $\gamma$ -Fe,Ni,Si phase ( $Fm-3m$ ,  $a = 3.58 \text{ \AA}$ ). FeCrB ( $Fddd$ ,  $a = 14.57 \text{ \AA}$ ,  $b = 7.32 \text{ \AA}$  and  $c = 4.22 \text{ \AA}$ ) matches a B-rich A3-phase. A3 and A4, due too very slight differences, are not distinguishable in XRD results, similarly to the EPMA study. Finally, A6 is supposedly a BCC (Body Centered Cubic) phase ( $Im-3m$ ,  $a = 2.86 \text{ \AA}$ ). Low intensity of its peak could be justified by its small size and a position far below the surface of the coating. The correct attribution of the FCC (Face Centered Cubic), BCC and  $P2_13$  phase to the A1, A2 and A6 phases, that have relatively close atomic compositions, was confirmed by a supplementary EBSD analysis (Fig. 5). Nonetheless, numerous peaks of this diffractogram (Fig. 4a) were not attributed.

**Table 4** Composition (at.%) obtained by EPMA of the phases observed in coating A and coating B (according to Figs. 2 and 3)

Phase	Si	P	Cr	Mn	Fe	Ni	Mo	V	B
A1	18.8		7.7		55.0	17.8	0.4	0.3	
A2	13.9		8.0	0.6	59.2	18.4	0.3	0.2	
A3/A4			31.5	0.1	33.9	1.1	0.7	0.7	32.0
A6	14.9		4.9		62.5	17.3	0.2	0.1	
B1	4.3	28.8	31.4	0.1	14.6	20.6			
B2	15.0	2.0	46.8	0.1	3.2	32.9			
B3	11.9	0.3	13.0	0.1	32.7	42.0			
B4	19.3	6.8	11.7	0.3	10.2	51.7			

**Fig. 4** XRD patterns of coatings A (a) and B (b)

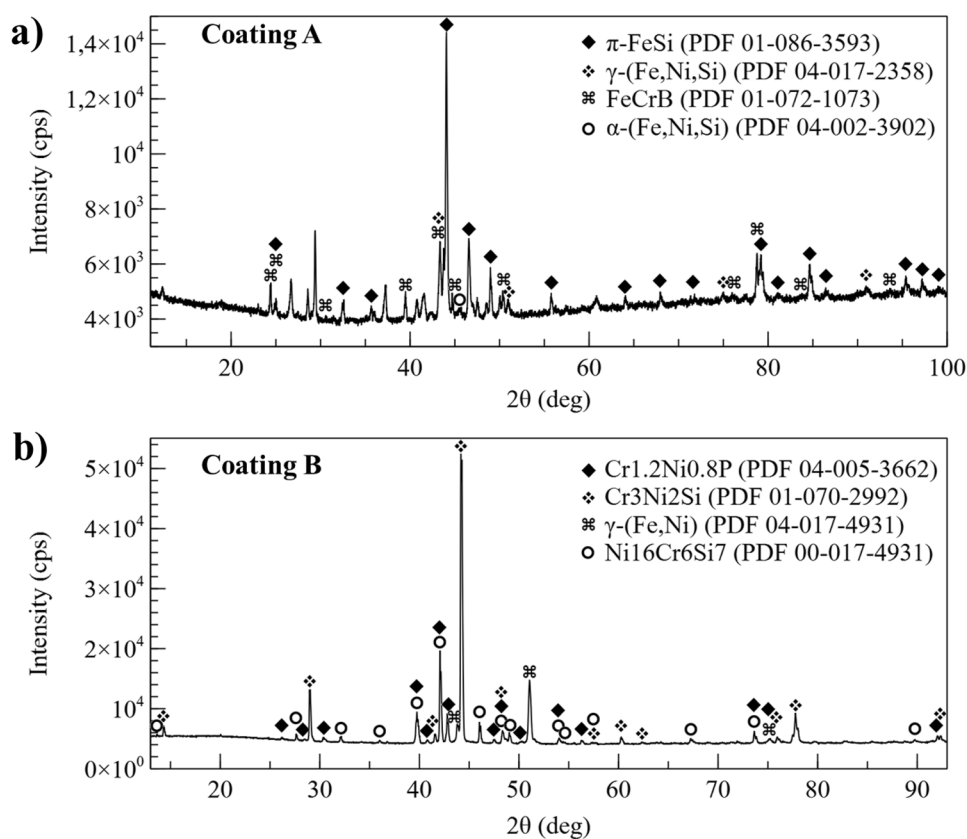
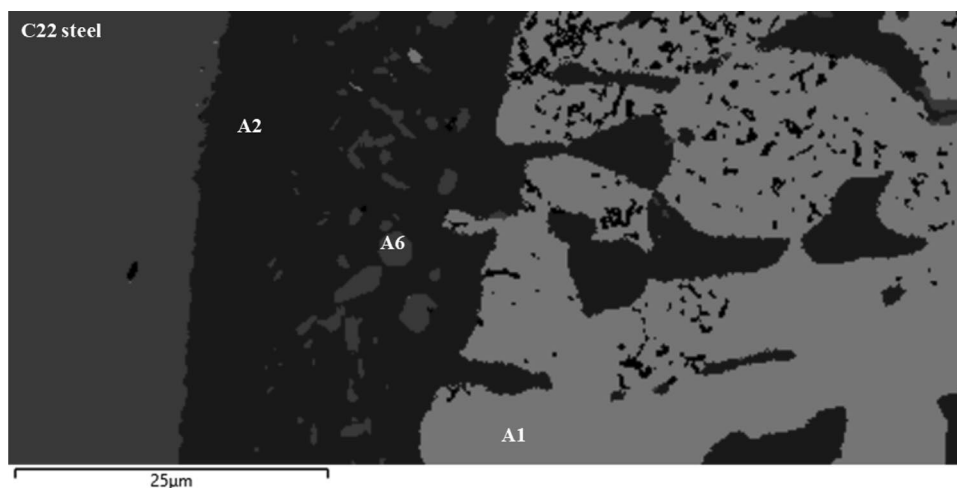


**Fig. 5** EBSD image of the coating A: BCC (medium grey), FCC (dark grey) and P<sub>2,3</sub> (light grey) phases. The phase on the left is the steel substrate



They are presumably related to the presence of Nb- and Mo-rich inclusions, which are scarce, dispersed in the coating and differ in composition from one another, as seen in the EPMA investigation. As a result, they are challenging to characterize with XRD. However, they are present in the coating, and thus visible on the SEM image.

Furthermore, all the peaks of the B-coating's diffractogram (Fig. 4b) were attributed to one of 4 crystal phases. Cr<sub>1,2</sub>Ni<sub>0,8</sub>P phase of Pnma space group ( $a = 5.89 \text{ \AA}$ ,  $b = 3.52$

$\text{\AA}$  and  $c = 6.76 \text{ \AA}$ ) corresponds well with P-rich B1 phase, whereas B2 phase, which has a high Cr content, match well with Cr<sub>3</sub>Ni<sub>2</sub>Si (Fd-3ms,  $a = 10.62 \text{ \AA}$ ). The  $\gamma$ -(Fe,Ni) and Ni<sub>16</sub>Cr<sub>6</sub>Si<sub>7</sub> have the same space group Fm-3m ( $a = 3.57 \text{ \AA}$  and  $a = 11.12 \text{ \AA}$  respectively). Regarding the EPMA results of B3 and B4 phase, B4 corresponds to Ni<sub>16</sub>Cr<sub>6</sub>Si<sub>7</sub> with its higher Si and Ni content. The proportion does not match perfectly; therefore, the lattice parameter was adjusted. Consequently,  $\gamma$ -(Fe,Ni) suits the B3 phase.

The elemental compositions of the two coatings are similar, each being characterized by their corresponding light element (B, P). Additionally, the slurry process leads to the diffusion of iron in the coating. The difference of the iron content in final coatings comes from the initial chemical composition being distinct in each powder, and thus diverse diffusion gradients.

The differences in the composition do not influence the presence of cracks in each coating. However, their microstructures, despite the fact that both coatings contain an important fraction of the FCC phase, are different. Each coating has one phase corresponding to their light elements and remaining phases do not match one another.

### 3.3 Weight loss during galvanizing cycles

The results of weight loss per surface unit in contact with the liquid zinc alloy are presented on Fig. 6. The corrosion rate is described by the slope of the trendline. It is observed that the C22 carbon steel corrodes the most rapidly with  $0.44 \text{ mg.cm}^{-2}.\text{min}^{-1}$  in the first part of the curve and  $0.66 \text{ mg.cm}^{-2}.\text{min}^{-1}$  in the last part. The 316 L stainless steel presents a better resistance with an average weight loss rate of  $0.17 \text{ mg.cm}^{-2}.\text{min}^{-1}$ . The coated steel samples with only  $6 \text{ mg.cm}^{-2}$  of weight loss after 20 cycles present a better resistance than stainless steel ( $10 \text{ mg.cm}^{-2}$  of weight loss). However, if the weight loss is around zero for the first cycles, after the 9th cycle the weight of the sample decreases at the same rate that for the stainless steel. That probably means that the coating is resistant during the 9th firsts cycles and after, its corrosion presents the same rate than the stainless steel up to more than 20 cycles. According to the initial thickness of the

coating (A =  $80 \mu\text{m}$ ; B =  $45 \mu\text{m}$ ) and the average density of the coating material ( $8 \text{ g.cm}^{-3}$ ), the maximum length live is estimated to 368 min or 122 cycles for coating A and 207 min or 68 cycles for coating B.

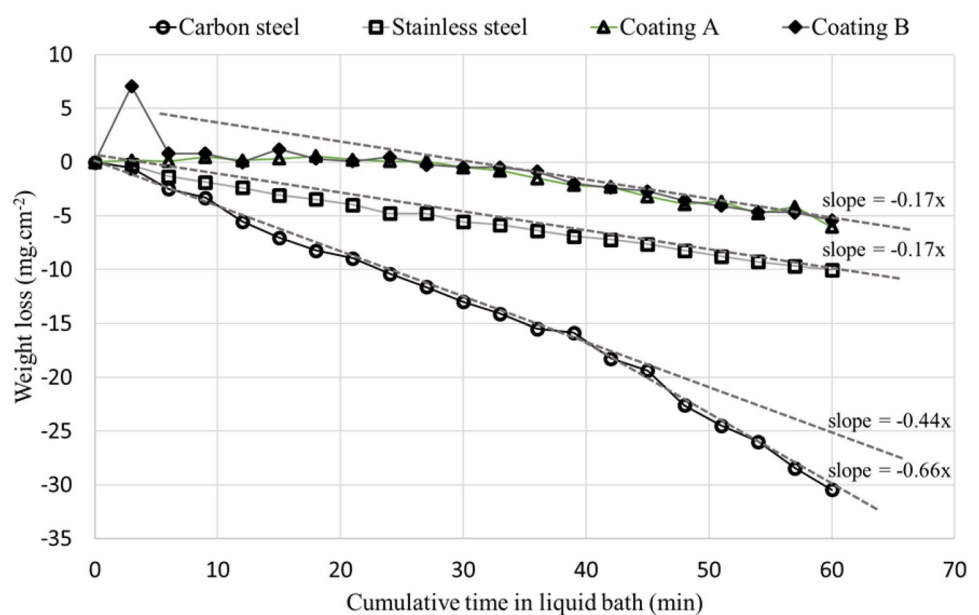
Despite different compositions, both coatings have the same effect on the corrosion behavior in liquid zinc. Therefore, light elements like bore and phosphorus do not seem to influence it. Also, cracks and impurities present in the coating A do not have any damaging effect on the corrosion resistance. Presence of common elements like Si or Cr or of the FCC phase could be suspected to be responsible of the protective effect.

## 4 Discussion

Commonly used for continuous galvanizing, ceramic coatings [7, 9, 25] have the thermal shock resistance too low to be used in batch galvanizing, where parts are quickly moved from room temperature environment into zinc bath at  $450 \text{ }^\circ\text{C}$ . The slurry process leads to the coatings A and B with interdiffusion layer, as iron present in the coating's phases come from the steel and not from the powder. That structure is probably the root of their good thermal shock resistance, as no significant damage of coatings was observed after 20 galvanizing cycles.

The preparation and thermal treatment for both compositions of coatings are the same, however the particle sizes are not strictly identical in the two powders. The difference in the rheology of both slurries may be the reason that the coating A is thicker than the coating B. The role of the thickness on the service life and corrosion behavior of coatings is yet to be studied. Current

**Fig. 6** Weight loss of the studied materials for 3 min galvanizing cycles





results are suggesting that the corrosion rate is linear, thus the service life should be proportional to the thickness. If the corrosion is not completely uniform, however, more complicated deterioration mechanisms may be in play.

Dissolution of steel by liquid zinc is similar in batch and continuous galvanizing. The mechanisms of limitation of corrosion can be either of the presence of the phases resistant to dissolution [7–9] or the presence of inert oxide layers [7, 25]. The mechanism of protection in case of the coatings A and B needs a further study. Assuming that those are the oxides that form on the surface, they need to show the additional resistance to the deoxidation by flux. Following the Ellingham diagram,  $\text{SiO}_2$  and  $\text{CrO}_3$  are more stable than  $\text{Fe}_3\text{O}_4$  which is to be deoxidized by the flux. Therefore, those are the compounds suspected to form on the surface on the coating and to be responsible for limiting the dissolution of steel. Both coatings and 316 L stainless steel contain elements which promote the formation of passive oxide layers. Moreover, they all also include a significant fraction of a FCC phase. According to Xu et al. [26], the high compacity of this phase could limit the diffusion of zinc into steel. Those two characteristics may explain the parallels in the corrosion rate of the stainless steel and the coatings, but further study is necessary to fully understand the mechanisms of corrosion due to the complexity of the phase composition of coatings.

Stainless steel is resistant to the corrosion in both galvanizing processes, however, in batch galvanizing, the degradation is highly accelerated. As states Wang et al. [12], whose work tested corrosion in flowing zinc, the corrosion rate of 316 L stainless steel at 460 °C is of  $50 \mu\text{m}\cdot\text{h}^{-1}$ , whereas in the case of this study, the loss of  $10 \text{ mg}\cdot\text{cm}^{-2}$  can be translated to  $780 \mu\text{m}\cdot\text{h}^{-1}$ . The difference may come from the two steps that are added to the batch galvanizing in comparison to the continuous process – cyclic fluxing and stripping. The stripping step is responsible for accelerated weight loss in comparison to the continuous process, as any portion of Fe–Zn intermetallics formed is dissolved and therefore revealing the fresh surface to be attacked by liquid zinc. Because of that, the performance of protective coatings used in batch galvanizing, such as coatings A and B, cannot be compared directly with the values obtained in the studies on continuous galvanizing, because they will consequently seem better [8, 9, 27].

At last, the coatings A and B do not seem sensible to the presence of hydrogen produced massively during the stripping step, that is responsible for the intergranular cracking of AHSS steels during electro galvanizing [28, 29], as no intergranular crack was observed in the samples.

## 5 Conclusion

Coatings studied in this article were synthesized by slurry process in order to protect steel from corrosion in liquid zinc during cyclic hot dip galvanization. Those complex materials composed of Fe, Cr, Ni, Si and light elements (boron for coating A, and phosphorus for coating B) were at first characterized through elemental and crystallographic analyses (EDX, EPMA, EBSD and XRD). Then, their performances were examined through cyclic corrosion tests, designed to imitate the cycles of batch galvanizing.

- Four main phases were detected in each coating:  $\pi$ -ferrosilicide, FCC, BCC and FeCrB in coating A and  $\text{Cr}_{1.2}\text{Ni}_{0.8}\text{P}$ ,  $\text{Cr}_3\text{Ni}_2\text{Si}$ ,  $\text{Ni}_{16}\text{Cr}_6\text{Si}_7$  and FCC in coating B.
- The FCC phases seem to stop the crack propagation in both coatings.
- Weight loss in tested materials increases linearly with the time spent in the liquid zinc during further cycles.
- The coatings improve considerably the corrosion resistance in comparison to the corrosion for the carbon steel without coating.
- During the 8 first 3-minute cycles of galvanization, the no corrosion of the coatings is observed and from the 9th to the 20th, the corrosion rate is the same that for the 316 L stainless steel. Therefore, those coated samples present higher time of life in comparison with the 316 L steel.
- Liquid zinc corrosion in cyclic galvanizing is up to 16 times higher than in continuous process for the same immersion time.

It is hypothesized that the coating's high content of silicon, that can form a nanometric oxide layer on the surface, is responsible for the corrosion protection due to lower liquid metal wettability of the oxide compared to the metal surface. Therefore, a better understanding of the mechanisms behind those protective properties could be provided by a further study of the extreme surface composition and its possible alterations throughout different stages of galvanization cycles.

**Acknowledgements** For his strong implication to this study, the authors thank David WARICHET. The electron probe microanalyser (EPMA) facility in Lille (France) is supported by the ERDF. The Chevreul Institute is thanked for its help in the development of this work through the ARCHI-CM project supported by the "Ministère de l'Enseignement Supérieur de la Recherche et de l'Innovation", the region "Hauts-de-France", the ERDF program of the European Union and the Métropole Européenne de Lille. This project is partially financed by the region "Haut-de-France".

**Funding** The authors have not disclosed any funding.

## Declarations

**Conflict of interest** The authors declare that they have no known competing financial interests or personal relationships that could have appeared to influence the work reported in this paper.

**Open Access** This article is licensed under a Creative Commons Attribution 4.0 International License, which permits use, sharing, adaptation, distribution and reproduction in any medium or format, as long as you give appropriate credit to the original author(s) and the source, provide a link to the Creative Commons licence, and indicate if changes were made. The images or other third party material in this article are included in the article's Creative Commons licence, unless indicated otherwise in a credit line to the material. If material is not included in the article's Creative Commons licence and your intended use is not permitted by statutory regulation or exceeds the permitted use, you will need to obtain permission directly from the copyright holder. To view a copy of this licence, visit <http://creativecommons.org/licenses/by/4.0/>.

## References

1. Kergar Neghab A, Hrymak AN, Goodwin FE (2015) In: 10th International Conference on Zinc and Zinc Alloy Coated Steel Sheet (Galvatech 2015), AIST, Toronto, Canada
2. Zhang K, Tang NY, Goodwin F (2007) Reaction of 316L stainless steel with a galvanizing bath. *J of Mater Sci* 42:9736–9745. <https://doi.org/10.1007/s10853-007-1978-y>
3. Hardy Y, Dubois M, Bertrandie JJ, Saint-Raymond H (2007) In: 7th International Conference on Zinc and Zinc Alloy Coated Steel Sheet (Galvatech '07), Osaka, Japon
4. Perrot P, Tissier JC, Dauphin JY (1992) Stable and metastable equilibria in the Fe–Zn–Al system at 450°C. *Z. für Metallkunde*. 83(11):786–790. <https://doi.org/10.1515/ijmr-1992-831104>
5. Yamaguchi S, Makino H, Sakatoku A, Iguchi Y (1995) In: International Conference on Zinc and Zinc Alloy Coated Steel Sheet (Galvatech '95), Chicago, IL
6. Tang NY, Su X (2002) On the ternary phase in the zinc-rich corner of the Zn–Fe–Al system at temperatures below 450°C. *Metall Mater Trans A* 33A:1559–1561. <https://doi.org/10.1007/s11661-002-0078-5>
7. Matthews S, James B (2010) Review of thermal spray coating applications in the steel industry: part 2 - zinc pot hardware in the continuous galvanizing line. *J Therm Spray Technol* 19:1277–1286. <https://doi.org/10.1007/s11666-010-9519-7>
8. Ma S, Xing J, Fu H, Yu D, Zhang J, Li Y, Zhang Z, Zhu B, Ma S (2011) Interfacial morphology and corrosion resistance of Fe–B cast steel containing chromium and nickel in liquid zinc. *Corros Sci* 53:2826–2834. <https://doi.org/10.1016/j.corsci.2011.05.020>
9. Ren X, Mei X, She J, Ma J (2007) Materials resistance to liquid zinc corrosion on surface of sink roll. *J Iron Steel Res Int* 14(5):130–136. [https://doi.org/10.1016/S1006-706X\(08\)60066-7](https://doi.org/10.1016/S1006-706X(08)60066-7)
10. Zhang J, Deng C, Song J, Deng C, Liu M, Zhou K (2013) MoB–CoCr as alternatives to WC–12Co for stainless steel protective coating and its corrosion behavior in molten zinc. *Surf Coat Technol* 235:811–818. <https://doi.org/10.1016/j.surfcoat.2013.08.052>
11. Wang Y, Xing J, Ma S, Zheng B, Fu H, Liu G (2016) Interfacial morphologies and erosion–corrosion behavior of directional Fe–3.5 wt% B steel in flowing liquid Zn containing 0.30 wt% Al. *Corros Sci* 112:25–35. <https://doi.org/10.1016/j.corsci.2016.07.007>
12. Wang Y, Xing J, Ma S, Zheng B, Fu H, Liu G, Yang D, Bai Y (2016) Interface characterization and erosion–corrosion behavior of directional Fe–3.5wt% B steel in flowing liquid zinc at various temperatures. *Corros Sci* 104:260–268. <https://doi.org/10.1016/j.corsci.2015.12.018>
13. Wang Y, Xing J, Fu H, Liu Y, Zheng K, Ma S, Jian Y (2018) Interfacial morphology and corrosion–wear behavior of cast Fe–3.5 wt% B steel in liquid zinc. *Corros Sci* 131:290–299. <https://doi.org/10.1016/j.corsci.2017.12.003>
14. Wang W, Lin J, Wang Y, Chen G (2007) The corrosion of intermetallic alloys in liquid zinc. *J Alloy Compd* 428:237–243. <https://doi.org/10.1016/j.jallcom.2006.02.072>
15. Fang X, Wang Y, Zhang Y, Feng S, Du J, Liu D, Ouyang T, Suo J, Cai S (2016) Improving the corrosion resistance of Fe–21Cr–9Mn alloy in liquid zinc by heat treatment. *Corros Sci* 111:362–369. <https://doi.org/10.1016/j.corsci.2016.05.018>
16. Reignier C, Lee D, De Wet D (2002) In: ITSC 2002 International Thermal Spray Conference, Essen, Germany
17. Stern KH (1996) Metallurgical and ceramic protective coatings, 1st edn. Chapman & Hall, Washington. [https://doi.org/10.1007/978-94-009-1501-5\\_8](https://doi.org/10.1007/978-94-009-1501-5_8)
18. Bianco R, Rapp RA (1993) Pack cementation aluminide coatings on superalloys: codeposition of Cr and reactive elements. *J Electrochem Soc* 140(4):1181. <https://doi.org/10.1149/1.2056219>
19. Meier GH, Cheng C, Perkins RA, Bakker W (1989) Diffusion chromizing of ferrous alloys. *Surf Coat Technol* 39:53–64
20. Sakidja R, Park JS, Hamann J, Perepezko JH (2005) Synthesis of oxidation resistant silicide coatings on Mo–Si–B alloys. *Scr Mater* 53(6):723–728. <https://doi.org/10.1016/j.scriptamat.2005.05.015>
21. Knittel S, Mathieu S, Portebois L, Drawin S, Vilasi M (2013) Development of silicide coatings to ensure the protection of Nb and silicide composites against high temperature oxidation. *Surf Coat Technol* 235:401–406. <https://doi.org/10.1016/j.surfcoat.2013.07.053>
22. Priceman S, Sama L (1967) Fused slurry silicide coatings for the elevated temperature oxidation of columbium alloys. *Metall Soc Conf* 41:959–982
23. Fauchais P, Montavon G (2010) Latest developments in suspension and liquid precursor thermal spraying. *J Therm Spray Technol* 19(1–2):226–239. <https://doi.org/10.1007/s11666-009-9446-7>
24. Bowden D, Krysiak Y, Palatinus L, Tsivoulas D, Plana-Ruiz S, Sarakinou E, Kolb U, Stewart D, Preuss M (2018) A high-strength silicide phase in a stainless steel alloy designed for wear-resistant applications. *Nat Commun* 9:1374. <https://doi.org/10.1038/s41467-018-03875-9>
25. Liberski P, Podolski P, Gierak A, Formanek B (1997) Interaction of liquid zinc with non-metallic coatings on steel. *Mater Sci Forum*. <https://doi.org/10.4028/www.scientific.net/MSF.251-254.693>
26. Xu J, Bright MA, Liu X, Barbero E (2007) Liquid metal corrosion of 316L stainless steel, 410 stainless steel, and 1015 carbon steel in a molten zinc bath. *Metall Mater Trans A* 38:2727–2736. <https://doi.org/10.1007/s11661-007-9320-5>
27. Xie X, Yin B, Yin F, Ouyang X (2021) Corrosion behavior of FeB–30 wt% Al<sub>0.25</sub>FeNiCoCr cermet coating in liquid zinc. *Coatings* 11:622. <https://doi.org/10.3390/coatings11060622>
28. McCarty ED, Wetzel D, Klobdanz B (1996) Hydrogen embrittlement in automotive fastener applications. *SAE Trans* 105:355–383
29. Khare A, Dwivedi SK, Vishwakarma M, Ahmed S (2018) Experimental Investigation of hydrogen embrittlement during coating process and effect on mechanical properties of high strength steel used for fasteners. *Mater Today Proc* 5(9):18707–18715. <https://doi.org/10.1016/j.matpr.2018.06.217>

**Publisher's Note** Springer Nature remains neutral with regard to jurisdictional claims in published maps and institutional affiliations.